16th World Congress in Computational Mechanics (WCCM)
21-26 July 2024, Vancouver, Canada
A. Korobenko, M. Laforet, S. Prudhomme, R. Vaziri (Eds)

ESTIMATION OF GRINDING CONTACT STIFFNESS AND DAMPING PARAMETERS USING HUNT-CROSSLEY FORCE MODEL AND UNCENTED KALMAN FILTER

QUOC-CUONG NGUYEN[1], VIET-HUNG VU*[1], AND MARC THOMAS[2]

[1] Department of Mechanical Engineering and Aerospace Engineering
Royal Military College of Canada, K7K 7B4, Kingston, Canada
*Email: viet-hung.vu@rmc-cmr.ca, Web page : https://www.rmc-cmr.ca/en

[2] Department of Mechanical Engineering,
École de technologie supérieur, H3C 1K3, Montréal, Canada
Email: marc.thomas@etsmtl.ca, Web page : https://www.etsmtl.ca/

Keywords: Contact stiffness, damping, flexible manipulators, Unscented Kalman Filter, contact force, Hunt-Crossley model.

Abstract. This paper introduces a novel approach that combines the Unscented Kalman Filter with the Hunt-Crossley force model to accurately estimate the stiffness and damping characteristics at the contact point of a grinding process conducted by a flexible manipulator. The Hunt-Crossley force model is proposed for the force contact considering the flexibility of the manipulator structure. It is written in a state form as a function of contact stiffness and damping. Leveraging the Unscented Transform to linearize the nonlinear measurement functions, the Unscented Kalman Filter effectively estimates and updates the stiffness and damping parameters based on the state model. This method is put into practice in a real grinding scenario employing a flexible manipulator. Its practicality and convenience make it a promising technique for estimating operational machining parameters and developing an efficient vibration control strategy for machining applications.

1 INTRODUCTION

Robotic machining offers a promising alternative to conventional machining tasks, thanks to its advantages including high flexibility, cost-effectiveness, and productivity. However, the relatively low stiffness of flexible robots can significantly impact their positioning accuracy, resulting in reduced machining quality and production efficiency. This issue becomes especially critical when the robot is tasked with highly dexterous and adaptable operations in diverse and uncertain conditions [1, 2]. Therefore, precise estimation of contact damping and stiffness is essential for the successful operation of robot-related tasks regarding explicit force control. Identifying the dynamic characteristics of the contact environment can greatly enhance the autonomy of the robot system [3-5]. Despite the considerable progress in robotic system research made possible by advanced software and powerful computer hardware, the modeling and control of constrained robotic operations remain challenging [6]. Extensive research has explored this area, and various approaches can be categorized based on the assumed contact models, methodologies, and the interaction control system, utilizing measured data. For instant, The Kevin-Voigt model [7] simplifies the relationship between contact bodies' penetration and contact force using a parallel arrangement of a linear spring and a viscous damper, with subsequent developments integrating surface dynamics and introducing related models like Maxwell [8] and Kelvin-Boltzmann [9]. Nonetheless, these linear models describe forces that do not correspond to their natural behavior, which can compromise the accuracy of estimation solutions and fall short in capturing the nonlinear characteristics of tool interaction [10, 11]. To precisely discern environmental and contact dynamics, focus has also shifted towards estimating parameters within nonlinear contact models. In the context of robotic tasks, energy dissipation during the contact process must be taken into consideration to accurately describe the nonlinear nature of the process [12] . Consequently, in the scope of this paper, we introduce an online algorithm that combines the nonlinear Hunt Crossley contact model [13] with the Unscented Kalman Filter [14] algorithm (UKF) to determine the contact parameters for a rigid single-point interaction. This proposed approach simplifies the implementation process and can be achieved through the utilization of unscented transformation. We have validated the method accuracy through experiments on the SCOMPI robot, conducted via a series of tests under varying grinding power conditions. The effectiveness and resilience of this parameter estimation approach were confirmed by contrasting it with a traditional Recursive Least Squares algorithm [15].

2 HUNT-CROSLEY FORCE MODEL

In this paper, since the specific task of a SCOMPI robot is grinding in contact with a stiff workpiece, the contact events thus consider only one contact point, and the manipulator end effector motion under grinding operation is in the normal direction to the workpiece. The Hunt Crosley concept will be utilized for a better demonstration of damping parameter, which aligns with physical intuition, and represents energy lost during impacts.

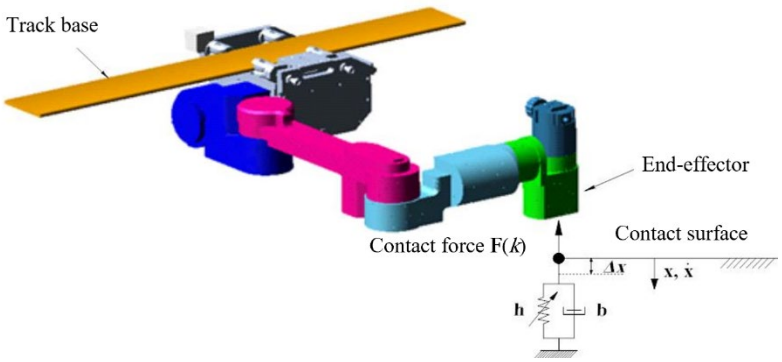

Figure 1: Single point contact of SCOMPI robot

A single-stage nonlinear contact model is presented in Figure 1. The nonlinear model is shown to have a good agreement with physical environments. The normal force $\mathbf{F}_{(k)}$ acting on a body is a function of displacement x of the body at the contact point. Within this framework, the spring symbolizes the elasticity of the contacting objects, while the damper represents energy dissipation at the contact point. Upon the manipulator's interaction with the environment, a contact force emerges. The H-C model enhances the linear amalgamation of the springs and dampers, resulting in the subsequent nonlinear equation:

$$\mathbf{F}_{(k)} = h\mathbf{x}^n(k) + b\mathbf{x}^n(k)\dot{\mathbf{x}}(k) \tag{1}$$

In this context, $\mathbf{F}_{(k)}$ denotes the contact force, $\mathbf{x}(k)$ signifies penetration into the environment and $\dot{\mathbf{x}}(k)$ represents the rate of displacement; h and b correspond to the environmental stiffness and damping parameters; $h\mathbf{x}^n(k)$ stands the nonlinear elastic force and $b\mathbf{x}^n(k)\dot{\mathbf{x}}(k)$ represents the nonlinear vicious force. The parameter n typically takes on positive scalar values, generally falling within the range of 1 to 2, and the material properties and geometric characteristics of the contact influence its variation. For b = 0, this model degenerates into Hert's model which is limited in application to modeling impacts which elastic deformation during hard contact [16].

By considering system noise $\boldsymbol{\varepsilon}(k)$, the model becomes:

$$\mathbf{F}_{(k)} = h\mathbf{x}^n(k) + b\mathbf{x}^n(k)\dot{\mathbf{x}}(k) + \boldsymbol{\varepsilon}(k) \tag{2}$$

To address the nonlinearity of equation (2), the Unscented Kalman Filter is introduced in the following section.

3 UNSCENTED KALMAN FILTER

In this section, we will outline a method employing the Unscented Kalman Filter (UKF) for the estimation of contact force parameters. The UKF method is based on the well-established principles of the Kalman filter. However, the approach utilizes the Unscented Transform (UT)

to calculate the prior probability distribution before executing the measurement update step. Unlike the Extended Kalman Filter (EKF), the UKF avoids relying on a linearization-based approximation for the nonlinear system. This model is constructed by a meticulous selection of Sigma points, designed to encapsulate the genuine mean and covariance of a specific distribution. Consequently, the UKF is capable of accurately estimating posterior means and covariances with a high degree of precision.

3.1 Unscented Transformation (UT)

The system state equation for online contact force characterization is based on the H-C model, and it is formulated as follows:

$$\begin{cases} \mathbf{X}_{k+1} = f\left(\mathbf{X}_k\right) + \mathbf{v}_k \\ \mathbf{F}_k = g\left(\mathbf{X}_k, \mathbf{x}_k, \dot{\mathbf{x}}_k\right) = h\mathbf{x}_k + b\mathbf{x}_k\dot{\mathbf{x}}_k + \mathbf{e}_k \end{cases} \tag{3}$$

where the system state is represented by $\mathbf{X}_k = \begin{bmatrix} h & b \end{bmatrix}^T$, f(.) denotes the system function and $\mathbf{v}_k$ represents the system noise or modeling error, $\mathbf{F}_k$ signifies the measurement of contact force, g(.) is the measurement function that defines the connection between the system state and the measurement, and $\mathbf{e}_k$ is measurement noise. We assumed that $\mathbf{v}_k$ and $\mathbf{e}_k$ are both uncorrelated Gaussian distributions, with the following statical characteristic.

$$\begin{aligned} \mathbf{E}\left[\mathbf{v}_k\mathbf{v}_s\right] &= \begin{cases} \mathbf{Q}_k & k = s \\ 0 & k \neq s \end{cases}; \\ \mathbf{E}\left[\mathbf{e}_k\mathbf{e}_s\right] &= \begin{cases} \mathbf{R}_k & k = s \\ 0 & k \neq s \end{cases} \quad \forall k, s \end{aligned} \tag{4}$$

Where $\mathbf{Q}_k$ and $\mathbf{R}_k$ represent the covariances of $\mathbf{v}_k$ and $\mathbf{e}_k$ respectively

Employing the Unscented Transform to linearize the nonlinear measurement function $g\left(\mathbf{X}_k, \mathbf{x}_k, \dot{\mathbf{x}}_k\right)$. These non-linear functions are embodied as discrete points known as sigma points, meticulously selected to capture their mean $\bar{\mathbf{X}}$ and covariance $\mathbf{P}_x$. Subsequently, these sigma points undergo a nonlinear transformation. This allows for derivation of the mean and covariance of the non-linearly transformed variable *X*, providing a statistical estimate.

The *L* dimension random variable *X* with mean $\bar{\mathbf{X}}$ and covariance $\mathbf{P}_x$ is portrayed using a matrix χ comprising 2*L*+1 sigma vector $\boldsymbol{\chi}_i$, and its respective weight W_i as follows:

$$\boldsymbol{\chi}_0 = \bar{\mathbf{X}} \tag{5}$$

$$\boldsymbol{\chi}_i = \bar{\mathbf{X}} + \left(\sqrt{L + \lambda}\mathbf{P}_x\right)_i ; \; i = 1, \ldots, L \tag{6}$$

$$\boldsymbol{\chi}_i = \overline{\mathbf{X}} - \left(\sqrt{L+\lambda \mathbf{P}_x}\right)_{i-L}; \; i = L+1,\ldots,2L \tag{7}$$

$$W_0^{(m)} = \lambda / \left(L+\lambda\right) \tag{8}$$

$$W_0^{(c)} = \lambda / \left(L+\lambda\right) + \left(1-\alpha^2+\beta\right) \tag{9}$$

$$W_i^{(m)} = W_i^{(c)} = 1/2\left(L+\lambda\right) \quad i = 1,\ldots,2L \tag{10}$$

where $\left(\sqrt{L+\lambda \mathbf{P}_x}\right)_i$ is the i^{th} row or column of the matrix representing the square root of $L+\lambda \mathbf{P}_x$, this can be achieved via Cholesky decomposition. $\lambda = \alpha^2\left(L+\varsigma\right) - L$ represents a scaling parameter, α controls the dispersion of the sigma points around $\overline{\mathbf{X}}$ and is typically assigned a small positive value, like 0.003, ς represents a secondary scaling parameter, typically set to zero, and β is employed to integrate prior knowledge about the distribution of X (For a Gaussian distribution, the optimal value for β is 2 [14]). $W_i^{(m)}$ and $W_i^{(c)}$ represent the weights associated respectively with the i^{th} means and covariance.

When each sigma vector undergoes a transformation via the nonlinear function, it results in:

$$\mathbf{F}_i = g\left(\boldsymbol{\chi}_i\right) \quad i = 0,\, 1,\, 2,\ldots,\, 2L \tag{11}$$

The means and covariance for **F** can be respectively determined as below:

$$\overline{\mathbf{F}} \approx \sum_{i=0}^{2L} W_i^{(m)} \mathbf{F}_i \tag{12}$$

$$\mathbf{P}_y \approx \sum_{i=0}^{2L} W_i^{(m)} \left(\mathbf{F}_i - \overline{\mathbf{F}}\right)\left(\mathbf{F}_i - \overline{\mathbf{F}}\right)^T \tag{13}$$

3.2 Implementation of UKF

Under these circumstances, the stochastic properties parameter is expanded to include the noise factors, effectively redefining it as the combination of the initial state, system perturbation, and measurement error:

$$\mathbf{X}_k^a = \begin{bmatrix} \mathbf{X}_k^T & \mathbf{v}_k^T & \mathbf{e}_k^T \end{bmatrix}^T \tag{14}$$

The following algorithms outline the execution of the UKF:

Initialization:

$$\widehat{\mathbf{X}}_0 = E\left[\mathbf{X}_0\right] \tag{15}$$

$$\mathbf{P}_0 = E\left[\left(\mathbf{X}_0 - \widehat{\mathbf{X}}_0\right)\left(\mathbf{X}_0 - \widehat{\mathbf{X}}_0\right)^T\right] \tag{16}$$

$$\widehat{\mathbf{X}}_0^a = E\left[\mathbf{X}_0^a\right] = \begin{bmatrix} \widehat{\mathbf{X}}_0^T & 0 & 0 \end{bmatrix} \tag{17}$$

$$\mathbf{P}_0^a = E\left[\left(\mathbf{X}_0^a - \widehat{\mathbf{X}}_0^a\right)\left(\mathbf{X}_0^a - \widehat{\mathbf{X}}_0^a\right)^T\right] = \begin{bmatrix} \mathbf{P}_0 & 0 & 0 \\ 0 & \mathbf{Q} & 0 \\ 0 & 0 & \mathbf{R} \end{bmatrix} \tag{18}$$

For k = 1, …, ∞, the computation of sigma points takes place:

$$\boldsymbol{\chi}_{k|k-1}^a = \left[\widehat{\mathbf{X}}_{k-1}^a \quad \widehat{\mathbf{X}}_{k-1}^a \pm \sqrt{\left(L+\lambda\right)\mathbf{P}_{k-1}^a}\right] \tag{19}$$

Time update equation:

$$\boldsymbol{\chi}_{k|k-1}^x = f\left(\boldsymbol{\chi}_{k|k-1}^x, \boldsymbol{\chi}_{k|k-1}^v\right) \tag{20}$$

$$\widehat{\mathbf{X}}_k^- = \sum_{i=0}^{2L} W_i^{(m)} \boldsymbol{\chi}_{i,k|k-1}^x \tag{21}$$

$$\mathbf{P}_k^- = \sum_{i=0}^{2L} W_i^{(c)} \left[\boldsymbol{\chi}_{i,k|k-1}^x - \widehat{\mathbf{X}}_k^-\right]\left[\boldsymbol{\chi}_{i,k|k-1}^x - \widehat{\mathbf{X}}_k^-\right]^T \tag{22}$$

$$\mathbf{F}_{k|k-1} = g\left(\boldsymbol{\chi}_{k|k-1}^x, \boldsymbol{\chi}_{k|k-1}^e\right) \tag{23}$$

$$\widehat{\mathbf{F}}_k^- = \sum_{i=0}^{2L} W_i^{(m)} \mathbf{F}_{i,k|k-1} \tag{24}$$

Measurement update equations:

$$\mathbf{P}_{\bar{f}_k \bar{f}_k} = \sum_{i=0}^{2L} W_i^{(c)} \left[\mathbf{F}_{i,k|k-1} - \widehat{\mathbf{F}}_k^-\right]\left[\mathbf{F}_{i,k|k-1} - \widehat{\mathbf{F}}_k^-\right]^T \tag{25}$$

$$\mathbf{P}_{x_k \bar{f}_k} = \sum_{i=0}^{2L} W_i^{(c)} \left[\boldsymbol{\chi}_{i,k|k-1}^x - \widehat{\mathbf{X}}_k^-\right]\left[\mathbf{F}_{i,k|k-1} - \widehat{\mathbf{F}}_k^-\right]^T \tag{26}$$

$$\mathbf{K} = \mathbf{P}_{x_k \bar{f}_k} \mathbf{P}_{\bar{f}_k \bar{f}_k}^{-1} \tag{27}$$

$$\widehat{\mathbf{X}}_k = \widehat{\mathbf{X}}_k^- + \mathbf{K}\left(\mathbf{F}_k - \widehat{\mathbf{F}}_k^-\right) \tag{28}$$

$$\mathbf{P}_k = \mathbf{P}_k^- + \mathbf{K}\mathbf{P}_{\bar{f}_k \bar{f}_k} \mathbf{K}^T \tag{29}$$

where $\boldsymbol{\chi}^a = \left[\left(\boldsymbol{\chi}^x\right)^T \quad \left(\boldsymbol{\chi}^v\right)^T \quad \left(\boldsymbol{\chi}^e\right)^T\right]^T$, L represents the dimension of the augmented variable, **Q** denotes the covariance of process noise, and **R** represents the covariance of measurement noise. And $W_i^{(m)}$ is the weight for the mean and $W_i^{(c)}$ is the weight for the covariance, as given by equation (10).

4 APPLICATIONS TO SCOMPI GRINDING

4.1 Description of the test structures

The subject of this research was a SCOMPI (Super COMPact Ireq) robot with a prismatic joint and five rotating joints. This robot was designed for automating on-site repair tasks, including grinding, welding, and hammer peening [17, 18]. Robotic grinding relies heavily on the interplay between the material removal process and the dynamic behavior of robots,

directly influencing both surface quality and material removal efficiency. Consequently, it is imperative to model the contact force, not only for controlling the material removal rate but also for guaranteeing task accuracy.

Figure 2: The configuration of the SCOMPI robot during the grinding process

Figure 2 illustrates the structure of the SCOMPI robot and its grinding performance on hydraulic turbines. Carrying out the grinding task at a high material removal rate (MRR) presents notable challenges for the robot, resulting in substantial vibratory responses at the end effector. In this study, we investigated further this aspect by modeling the robot and its contact environment. The goal is to identify the unknown contact properties at the contact point during grinding operations.

4.2 Measurement test setup

To illustrate the proposed contact identification concept, an experimental test was conducted using the SCOMPI robot. Figure 3 shows the robot during a grinding operation. To prevent the measurement of system disturbances, both a dynamometer and workpiece were securely attached to a sturdy table, which had a first natural frequency exceeding 1.2 kHz. Three PCB-352C34 piezoelectric sensors were installed at the robot's end effector to record the accelerations in X, Y, and Z directions.

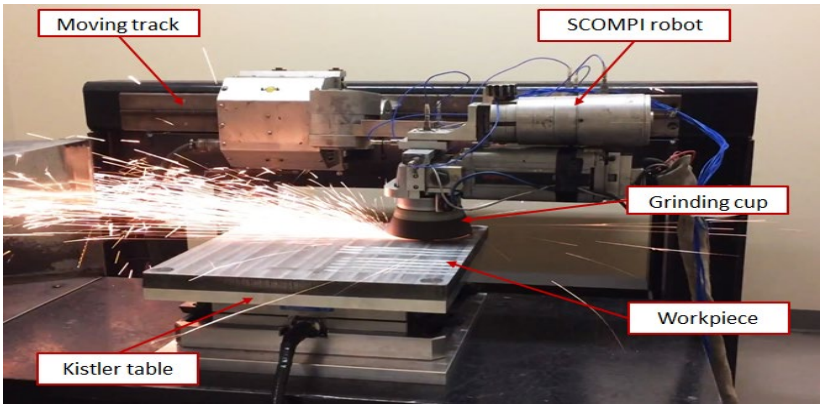

Figure 3: Experimentation conducted on the SCOMPI robot during grinding operations.

Meanwhile, a 3-axis Kistler dynamometer of type CH8408 was positioned beneath the workpiece to measure the grinding contact force. The measured accelerations were taken using the LMS data acquisition system for a continuous period of 20 seconds, and a sampling frequency of 512 Hz. The SCOMPI robot underwent a series of tests, configured for maximum stability to mitigate any adverse dynamic or vibration effects. Throughout all grinding experiments, motion control was employed to ensure precise tracking of the predefined path. Acceleration data were collected at various grinding paths to conduct a comprehensive investigation. The wheel's rotational speed was 3225 rpm, with an average axial grinding depth of 0.008 cm. Within the typical power range for grinding tasks, tests were conducted at five levels: 500W, 1500W, 2000W, 2500W, and 3000W. Single-groove experiments were executed along a length of 17.3 cm. The experiments were replicated three times to ensure measurement consistency. A workpiece made of hard steel AISI 1081, with a 71 HRC hardness and dimensions of 20.32 × 25.4 × 2.54 cm. When the end effector came into contact with the workpiece, impact forces were generated. This contact was then sustained until the robot was directed to disengage at t=20s. In this experiment, the identification algorithms were executed exclusively during the contact periods of the end effector.

Table 1: Grinding condition of SCOMPI robot

Experiment	Parameters
Grinder	Norton BlueFire 4NZ16QB-X406
Grinding cup diameter	12,7 (cm)
Workpiece material	AISI 1081
Workpiece dimensions	20.32 x 25.4 x 2.54 (cm)
Power	500, 1500, 2000, 2500, 3000 (W)
Speed	8 (cm/s)
Length of cut	16.2-18.5 (cm)
Width of cut	1-1.55 (cm)
Depth of cut	0.0158-0.00165 (cm)
Grinding direction	Normal direction
Rotation speed	3225 (rpm)
Angle of grinding cup	10 (degree)
Grinding condition	Dry grinding, single pass

5 COMPARE WITH LEAST SQUARE RESULTS

The vibration data collected during the grinding experiments were utilized to determine the contact force parameters for each power level, demonstrating the applicability of the proposed method in a real-world grinding scenario. The comparison results between the Recursive Least Squares (RLS) and Unscented Kalman Filter (UKF) methods under various grinding contact environments are shown in Figure 4. Table 2 presents the estimated contact damping

and stiffness directly obtained from the SCOMPI grinding experiment for different grinding powers of 500 W, 1500 W, 2000 W, 2500 W, and 3000 W.

Table 2: Estimated contact damping and stiffness results

P (W)	Estimated damping (N.s/m)		Estimated stiffness (N/m)	
	RLS	UKF	RLS	UKF
500	224.3	222.2	1.65×10^4	1.64×10^4
1500	268.5	257.8	1.79×10^4	1.79×10^4
2000	311.3	310.2	1.80×10^4	1.83×10^4
2500	353.5	346.8	1.99×10^4	1.97×10^4
3000	445.2	373.2	2.16×10^4	2.19×10^4

Throughout the experiment, it was noted that the estimated values for contact damping and contact stiffness increased with the power levels. A comparative analysis of two methods, Recursive Least Squares (RLS) [15] and Unscented Kalman Filter (UKF), was conducted under various grinding contact conditions. The ultimate findings are depicted in Figure 4, illustrating that the vibration and instability phenomena were considerably more pronounced when employing the RLS method compared to the UKF method.

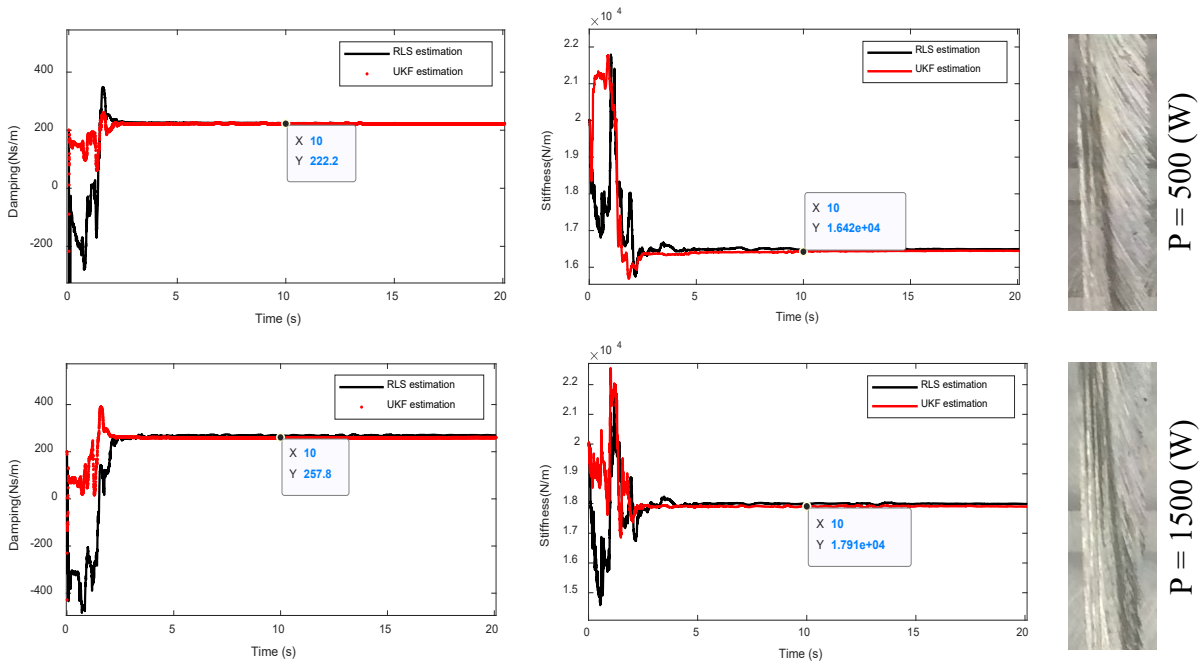

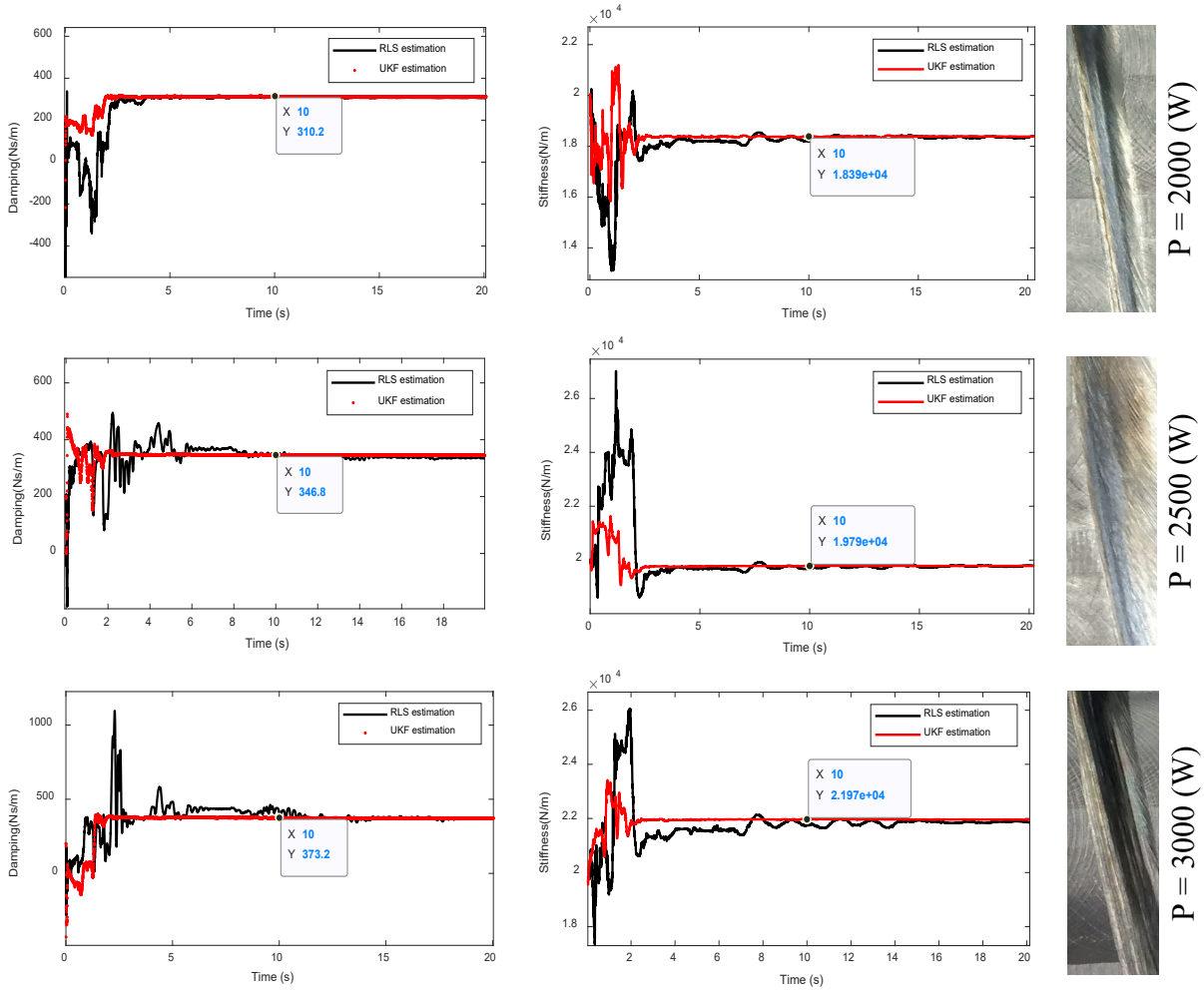

Figure 4: Estimated contact damping (left) and stiffness (right) with varying grinding power

Across a broader spectrum of initial conditions, it was anticipated that the UKF method would exhibit lower estimation errors when compared to the RLS method, highlighting the robustness and stability advantages of UKF over RLS. The stiffness estimation exhibited a shorter settling time compared to the damping estimation. The study revealed that increasing the power resulted in higher contact forces and could potentially lead to surface damage, such as burning. Therefore, it is suggested that the grinding power should be selected below 2000 (W) when operating the robot to avoid surface damage. Moreover, given the linear shape of each grinding path, it was reasonable to assume a single contact point. The contact forces, influenced by contact stiffness and damping, play a pivotal role in determining grinding performance indicators, such as workpiece quality and grinding accuracy.

6 CONCLUSIONS

This paper introduces a novel online identification technique that utilizes an enhanced version of the Kalman filter to estimate contact damping and stiffness parameters at the interaction

point between a robot and its surrounding environment. The study presents the outcomes of an identification process designed to estimate the parameters related to contact stiffness and damping in scenarios where robots interact with stiff environments. The utilization of the Unscented Kalman filter (UKF) with the Hunt Crossley nonlinear single-point contact model was introduced to characterize contact parameters between the grinding wheel and its environment. The experiment results and comparative analysis demonstrates that the proposed methodology, employing the Unscented Kalman filter (UKF), can effectively identify contact force parameters with significantly higher accuracy than traditional Recursive Least Squares estimation. Furthermore, online estimation of stiffness and damping can enhance force tracking in explicit force control systems.

REFERENCES

[1] G. M. Acaccia, P. C. Cagetti, M. Callegari, R. C. Michelini, and R. M. Molfino, "Modeling the impact dynamics of robotic manipulators," *IFAC Proceedings Volumes,* vol. 27, no. 14, pp. 559-564, 1994/09/01/ 1994, doi: https://doi.org/10.1016/S1474-6670(17)47366-6.

[2] N. Diolaiti, C. Melchiorri, and S. Stramigioli, "Contact impedance estimation for robotic systems," *IEEE Transactions on Robotics,* vol. 21, no. 5, pp. 925-935, 2005, doi: 10.1109/TRO.2005.852261.

[3] B.-O. Choi and K. Krishnamurthy, "Unconstrained and constrained motion control of a planar two-link structurally flexible robotic manipulator," *J. Field Robotics,* vol. 11, pp. 557-571, 1994.

[4] M. T. Grabbe, J. J. Carroll, D. M. Dawson, and Z. Qu, "Robust control of robot manipulators during constrained and unconstrained motion," in *Proceedings 1992 IEEE International Conference on Robotics and Automation*, 12-14 May 1992 1992, pp. 2146-2151 vol.3, doi: 10.1109/ROBOT.1992.219939.

[5] Q.-C. Nguyen, V.-H. Vu, and M. Thomas, "A Kalman filter based ARX time series modeling for force identification on flexible manipulators," *Mechanical Systems and Signal Processing,* vol. 169, p. 108743, 2022/04/15/ 2022, doi: https://doi.org/10.1016/j.ymssp.2021.108743.

[6] G. Gilardi and I. Sharf, "Literature survey of contact dynamics modelling," *Mechanism and Machine Theory,* vol. 37, no. 10, pp. 1213-1239, 2002/10/01/ 2002, doi: https://doi.org/10.1016/S0094-114X(02)00045-9.

[7] R. Lewandowski and B. Chorążyczewski, "Identification of the parameters of the Kelvin–Voigt and the Maxwell fractional models, used to modeling of viscoelastic dampers," *Computers & Structures,* vol. 88, no. 1, pp. 1-17, 2010/01/01/ 2010, doi: https://doi.org/10.1016/j.compstruc.2009.09.001.

[8] N. Sakamoto, M. Higashimori, T. Tsuji, and M. Kaneko, "An Optimum Design of Robotic Hand for Handling a Visco-elastic Object Based on Maxwell Model," *Proceedings 2007 IEEE International Conference on Robotics and Automation,* pp. 1219-1225, 2007.

[9] L. A. Sanchez, M. Q. Le, C. Liu, N. Zemiti, and P. Poignet, "The impact of interaction model on stability and transparency in bilateral teleoperation for medical applications," *2012 IEEE International Conference on Robotics and Automation,* pp. 1607-1613, 2012.

[10] D. W. Marhefka and D. E. Orin, "A compliant contact model with nonlinear damping for simulation of robotic systems," *IEEE Transactions on Systems, Man, and Cybernetics - Part A: Systems and Humans,* vol. 29, no. 6, pp. 566-572, 1999, doi: 10.1109/3468.798060.

[11] D. Zhang and B. Wei, "A review on model reference adaptive control of robotic manipulators," *Annual Reviews in Control,* vol. 43, pp. 188-198, 2017/01/01/ 2017, doi: https://doi.org/10.1016/j.arcontrol.2017.02.002.

[12] M. Machado, P. Moreira, P. Flores, and H. M. Lankarani, "Compliant contact force models in multibody dynamics: Evolution of the Hertz contact theory," *Mechanism and Machine Theory,* vol. 53, pp. 99-121, 2012/07/01/ 2012, doi: https://doi.org/10.1016/j.mechmachtheory.2012.02.010.

[13] K. H. Hunt and F. R. E. Crossley, "Coefficient of Restitution Interpreted as Damping in Vibroimpact," *Journal of Applied Mechanics,* vol. 42, no. 2, pp. 440-445, 1975, doi: 10.1115/1.3423596.

[14] S. J. Julier and J. K. Uhlmann, "Unscented filtering and nonlinear estimation," *Proceedings of the IEEE,* vol. 92, no. 3, pp. 401-422, 2004, doi: 10.1109/JPROC.2003.823141.

[15] Q.-C. N. Viet-Hung Vu, Marc Thomas, "Contact Stiffness and Damping Estimation by Hunt and Crossley Model - Application to Grinding Process," *Proceedings of the Canadian Society for Mechanical Engineering International Congress 31st".* Annual Conference of the Computational Fluid Dynamics Society of Canada, CSME/CFD2024, 2024.

[16] S. Muthukumar and R. Desroches, "A Hertz contact model with non-linear damping for pounding simulation," *Earthquake Engineering & Structural Dynamics,* vol. 35, pp. 811-828, 06/01 2006, doi: 10.1002/eqe.557.

[17] Q.-C. Nguyen, V.-H. Vu, and M. Thomas, "ARX model for experimental vibration analysis of grinding process by flexible manipulator," in *Surveillance, Vishno and AVE conferences*, Lyon, France, 2019-07-08 2019, https://hal.science/hal-02190280/document

[18] Q.-C. Nguyen, V.-H. Vu, and M. Thomas,, "Optimal ARMAX Model Order Identification of Dynamic Systems," *London Journal of Engineering Research,* vol. 22, no. 1, pp. 1-22, 04/11 2022. [Online]. Available: https://journalspress.uk/index.php/LJER/article/view/407.